



Iron doped graphitic carbon nitride with peroxidase like activity for colorimetric detection of sarcosine and hydrogen peroxide

Xiaoxue Xi¹ · Xu Peng¹ · Chengyi Xiong¹ · Deyao Shi² · Junlun Zhu¹ · Wei Wen¹ · Xiuhua Zhang¹ · Shengfu Wang¹

Received: 17 February 2020 / Accepted: 2 June 2020 / Published online: 12 June 2020
© Springer-Verlag GmbH Austria, part of Springer Nature 2020

Abstract

The successful synthesis is reported of Mn, Fe, Co, Ni, Cu-doped g-C₃N₄ nanoflakes via a simple one-step pyrolysis method, respectively. Among them, the Fe-doped g-C₃N₄ nanoflakes exhibited the highest peroxidase-like activity, which can be used for colorimetric detection of hydrogen peroxide (H₂O₂) and sarcosine (SA), within the detection ranges of 2–100 μM and 10–500 μM and detection limits of 1.8 μM and 8.6 μM, respectively. The catalytic mechanism of the Fe-doped g-C₃N₄ nanoflake was also explored and verified the generation of hydroxyl radical (•OH) through fluorescence method. It is believed that the Fe-doped g-C₃N₄ nanoflakes as enzyme mimics will greatly promote the practical applications in a variety of fields in the future including biomedical science, environmental governance, antibacterial agent, and bioimaging due to their extraordinary catalytic performance and stability.

Keywords Nanozyme · Fe-doped g-C₃N₄ nanoflakes · Peroxidase-like activity · Colorimetric sensors · Sarcosine detection · H₂O₂ detection

Introduction

As we know that the natural enzymes in the organism play a pivotal role in accelerating metabolism and promoting all life-related chemical reactions completed smoothly. Nonetheless, nanozymes possess many inimitable merits compared with the natural enzymes, such as lower cost, easier to synthesize, excellent stability, and

high resistance to acid or alkali, which have attracted many researchers in various fields devote to research them [1]. Especially some functionalized metal composite materials including metal and metal oxide nanoparticles [2], metal and carbon-based nanomaterials [3], metal clusters [4], metal sulfides [5], and metal-organic frameworks (MOFs) [6], which have been discovered possessing excellent peroxidase activity. Notably, due to the complex and cumbersome synthesis steps of MOFs-based nanomaterials, expensive raw materials of noble metals-based nanomaterials, lower activity of metalloid-based nanomaterials, and poor specificity, the novel materials with peroxidase-like activity have restricted the development and application of nanozymes to some extent. To overcome these shortcomings and broaden their application areas, Zhang's group synthesized a novel modifiable Au@BSA nanoparticle with a noble metal of gold [7], which improved the peroxidase-like activity significantly and had been used for the nonenzymatic colorimetric detection of glucose. Liu's group dedicated to study molecularly imprinted polymers of Fe₃O₄ inorganic nanozymes with extraordinary peroxidase-like activity and solved an inherent issue of nanozyme lacking of specificity [8]. Therefore, in terms of the development status of nanozymes, there is room

Electronic supplementary material The online version of this article (<https://doi.org/10.1007/s00604-020-04373-w>) contains supplementary material, which is available to authorized users.

✉ Wei Wen
wenwei@hubu.edu.cn

✉ Shengfu Wang
wangsf@hubu.edu.cn

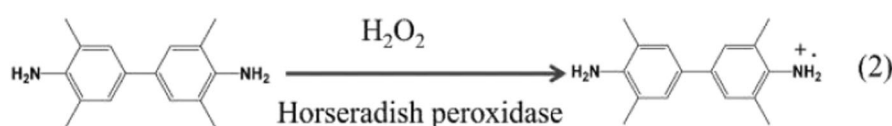
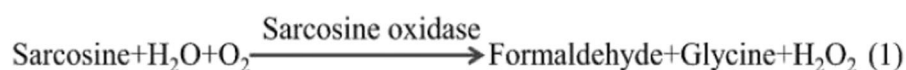
¹ State Key Laboratory of Biocatalysis and Enzyme Engineering, Ministry of Education Key Laboratory for the Synthesis and Application of Organic Functional Molecules, College of Chemistry and Chemical Engineering, Hubei University, Wuhan 430062, People's Republic of China

² Department of Orthopaedics, Union Hospital, Tongji Medical College, Huazhong University of Science and Technology, Wuhan 430022, People's Republic of China

for improvement in the development of highly peroxidase-like activity nanozymes with inexpensive raw materials and simple synthesis steps.

Graphite carbon nitride ($g\text{-C}_3\text{N}_4$), a polymer of two-dimensional (2D) nanomaterial with graphite-like structure, has aroused tremendous attentions in many fields including fluorometry [9] and photocatalysis [10]. Due to their nonnegligible advantages of excellent chemical stability, outstanding layered porous structure, adequate and cheap raw materials [11]. For instance, Wang et al. synthesized a type of $g\text{-C}_3\text{N}_4/\text{Pt}$ NPs nanocomposites by an ultrasonic-assisted chemical reduction step by step method to simulate the horseradish peroxidase activity and fabricated a sensitive colorimetric sensor to detect Hg^{2+} with outstanding selectivity [12].

Zhang et al. synthesized a kind of PdNPs/ $g\text{-C}_3\text{N}_4$ nanocomposites by a chemical reduction and high-temperature pyrolysis method to simulate the peroxidase activity [13], and developed an innovative dual-readout sensing platform for the detection of glucose. We can find that incorporating the noble metal element into $g\text{-C}_3\text{N}_4$ nanomaterials can not only improve their catalytic performances but also broaden their application fields. Even so, the synthesis of these $g\text{-C}_3\text{N}_4$ nanocomposites is usually accompanied with complicated and cumbersome steps. Therefore, developing a convenient method to synthesize the inexpensive metal doped- $g\text{-C}_3\text{N}_4$ nanozyme composite materials with enhanced stability is still a challenge.



Sarcosine, a kind of naturally occurring amino acid, plays a critical role in the diagnosis of prostate cancer (PCa) [14]. The level of sarcosine in urine or serum will elevate dramatically during prostate cancer progression and metastasis. In biological samples (urine and serum), the concentration of sarcosine can be measured between 1 and 20 μM [15]. Hydrogen peroxide (H_2O_2), as an important intermediate or product of many enzyme reactions, which has participated in many normal life activities processes in the human bodies, and many detection methods had been explored for the sensitive sensing of H_2O_2 [16–18]. In conclusion, it is considerable to develop an effective and sensitive colorimetric method to detect sarcosine in complex biological samples and make up for the deficiency of PCa diagnosis and treatment.

Herein, we proposed a convenient one-step pyrolysis method to synthesize novel Mn, Fe, Co, Ni, Cu-doped $g\text{-C}_3\text{N}_4$ nanoflakes with low-cost raw materials. Among them, Fe-doped $g\text{-C}_3\text{N}_4$ nanozyme has strong peroxidase activity and used for the colorimetric detection of sarcosine and H_2O_2 , respectively. Notably, sarcosine can be oxidized to generate H_2O_2 with the assistance of sarcosine oxidase (SOX), so we can determine the content of H_2O_2 to meet the purpose of quantitative and qualitative detection of sarcosine. And H_2O_2 can oxidize 3,3',5,5'-tetramethylbenzidine (TMB) effectively with the assistance of peroxidase, a colorimetric

platform for sensitive detection of H_2O_2 and sarcosine was fabricated involved with the oxidizing reaction between H_2O_2 and TMB. In our experiment, TMB was additionally added as a chromogenic reagent to generate an analytical signal. The kinetics of the catalytic reaction of Fe-doped $g\text{-C}_3\text{N}_4$ nanozymes was studied by TMB- H_2O_2 system, in which the Michaelis constant was 0.39 mM with H_2O_2 as substrate, and 0.16 mM with TMB, respectively. The results indicated that an innovative colorimetric sensing platform had been fabricated on the basis of the novel Fe-doped $g\text{-C}_3\text{N}_4$ nanoflakes nanozyme, and applied for sensitive detection of sarcosine and H_2O_2 , which have a tremendous potential in the application of environmental pollution prevention, medical diseases detection, and other unknown matrices in the near future.

Experimental

Synthesis of pure $g\text{-C}_3\text{N}_4$ nanoflakes and M (M = Mn, Fe, Co, Ni, Cu)-doped $g\text{-C}_3\text{N}_4$ nanoflakes

The reagents, characterization, and synthesis details of the Fe-doped $g\text{-C}_3\text{N}_4$ nanoflakes can be obtained from the electronic supplementary information (ESI). The Fe-doped $g\text{-C}_3\text{N}_4$

nanoflakes nanozyme were prepared according to a mature method [19] (Fig. 1). Firstly, we used iron (III) chloride hexahydrate ($\text{FeCl}_3 \cdot 6\text{H}_2\text{O}$) and dicyandiamide as raw materials and precursors, dicyandiamide experienced the process of condensation deamination and formed melamine, then continue to deamination to form melem polymer structure. Finally, melem comonomer units were connected by C-N-C bonds and formed C_3N_4 triazine skeleton structure. Fe^{3+} was doped to the g- C_3N_4 skeleton structure successfully under the high temperature of 500°C .

Kinetic analysis of Fe-doped g- C_3N_4 nanoflakes

The steady-state kinetic analysis was conducted in 3.0 mL HAc-NaAc buffer (pH 4.0) solutions containing $60 \mu\text{g mL}^{-1}$ Fe-doped g- C_3N_4 nanoflakes, and different concentrations of H_2O_2 or TMB ($0.1 \sim 0.7 \text{ mM}$). All reactions were performed in time scan mode by monitoring the variation of absorption spectra at 652 nm accompanied with a 400 S interval. The obtained results were well consistent with the Michaelis-Menten equation, K_m and V_{max} were calculated using the Lineweaver-Burk plots, respectively.

Detection of H_2O_2 and sarcosine

Sarcosine oxidase (SOX) was dissolved in KH_2PO_4 buffer (pH 8.2) to prepare different concentrations of SOX solution, the reagent was prepared fresh and chilled at 4°C . Then an equal volume of SOX (65 U/mL , $50 \mu\text{L}$) and sarcosine solution with different concentrations were mixed and incubated for 1 h at 37°C . After that, TMB and catalyst material were added to the above reaction system, HAc-NaAc (pH 4.0) solution was used as a buffer solution, and the ultimate volume of the solution was 3.0 mL as total, obtained 1.0 mM TMB, $30 \mu\text{g mL}^{-1}$ nanozyme, the absorption peaks at 652 nm of the reacted solution was measured by ultraviolet-visible (UV-Vis) spectrophotometry.

Results and discussion

Characterization of Fe-doped g- C_3N_4 nanoflakes

The transmission electron microscopy (TEM) images depicted that the nanoflakes were composed of high-density

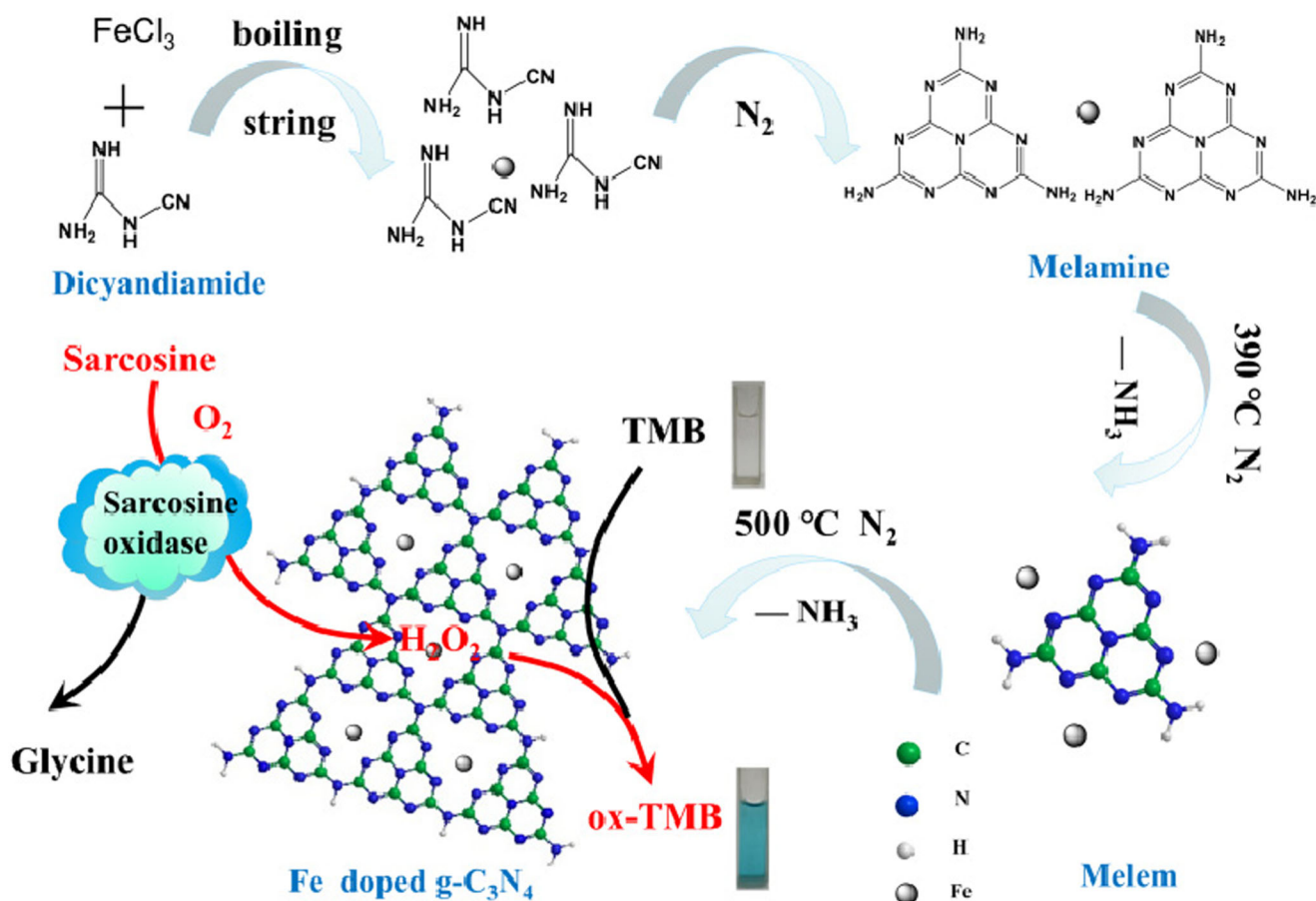


Fig. 1 Schematic diagram of Fe-doped g- C_3N_4 nanoflakes was constructed with dicyandiamide and FeCl_3 , and colorimetric detection of sarcosine and H_2O_2 based on sarcosine oxidase and Fe-doped g- C_3N_4 nanoflakes as peroxidase mimetic

interconnected layered structure, including a smooth paper-like stacking sheet structure (Fig. 2a and Fig. S1). The high-resolution TEM (HR-TEM) image showed that the lattice fringes with a spacing of 0.329 nm attributed to the classic (002) plane of $g\text{-C}_3\text{N}_4$ (Fig. 2b) [20, 21], which was in well agreement with the XRD patterns results of Fe-doped $g\text{-C}_3\text{N}_4$ nanoflakes. In addition, atomic force microscope (AFM) (Fig. S2), high-angle annular dark-field scanning TEM (HAADF-STEM) and elemental mapping were also accomplished to investigate the homogeneous distribution of Fe, C, and N in Fe-doped $g\text{-C}_3\text{N}_4$ nanoflakes (Fig. S3b and Fig. S3c-f). In addition, the HR-TEM, HAADF-STEM, and EDS elemental mapping of other metals (Mn, Co, Ni, Cu)-doped $g\text{-C}_3\text{N}_4$ nanoflakes were also conducted to further explore the morphology and element distribution (Fig. S4-S7). The discussion details can be found in the ESI.

To investigate the crystalline structure and purity of the different metals M-doped $g\text{-C}_3\text{N}_4$ (M = Mn, Fe, Co, Ni, Cu) nanoflakes, XRD was conducted to observe the phase structure of the nanoflakes (Fig. 2c). Two apparent diffraction peaks of $g\text{-C}_3\text{N}_4$ nanoflakes observed at 13.2° and 27.4°

could be ascribed to the (100) and (002) plane, the peak appears at 13.2° indexed as the (100) plane equivalent to the planar configuration of tri-s-triazine units [22]. Another predominant peak around 27.4° reveals the characteristic of interlayer accumulation of aromatic units of CN. Note here that after the incorporation of metals into $g\text{-C}_3\text{N}_4$, two apparent absorption peaks at 13.2° and 27.4° can still be observed clearly, the intensity of the peaks is weakened to some extent as a result of the incorporation of metals. The FT-IR spectrum was also performed to investigate the functional groups of the prepared nanoflakes (Fig. 2d). The pronounced several absorption bands between 1400 cm^{-1} and 1650 cm^{-1} can be ascribed to the typical stretching vibrations of the aromatic nucleus of C=N and C-N bonds. And the absorption bands in the range of $1230\text{--}1400\text{ cm}^{-1}$ correspond to the stretching vibrations of C-NH-C structure. The apparent absorption band at 806 cm^{-1} can be attributed to the triazine units. The broad absorption peak at 3400 cm^{-1} approximately can be associated with the stretching vibrations of N-H and O-H groups owing to the surface-absorbed H_2O molecules [22, 23].

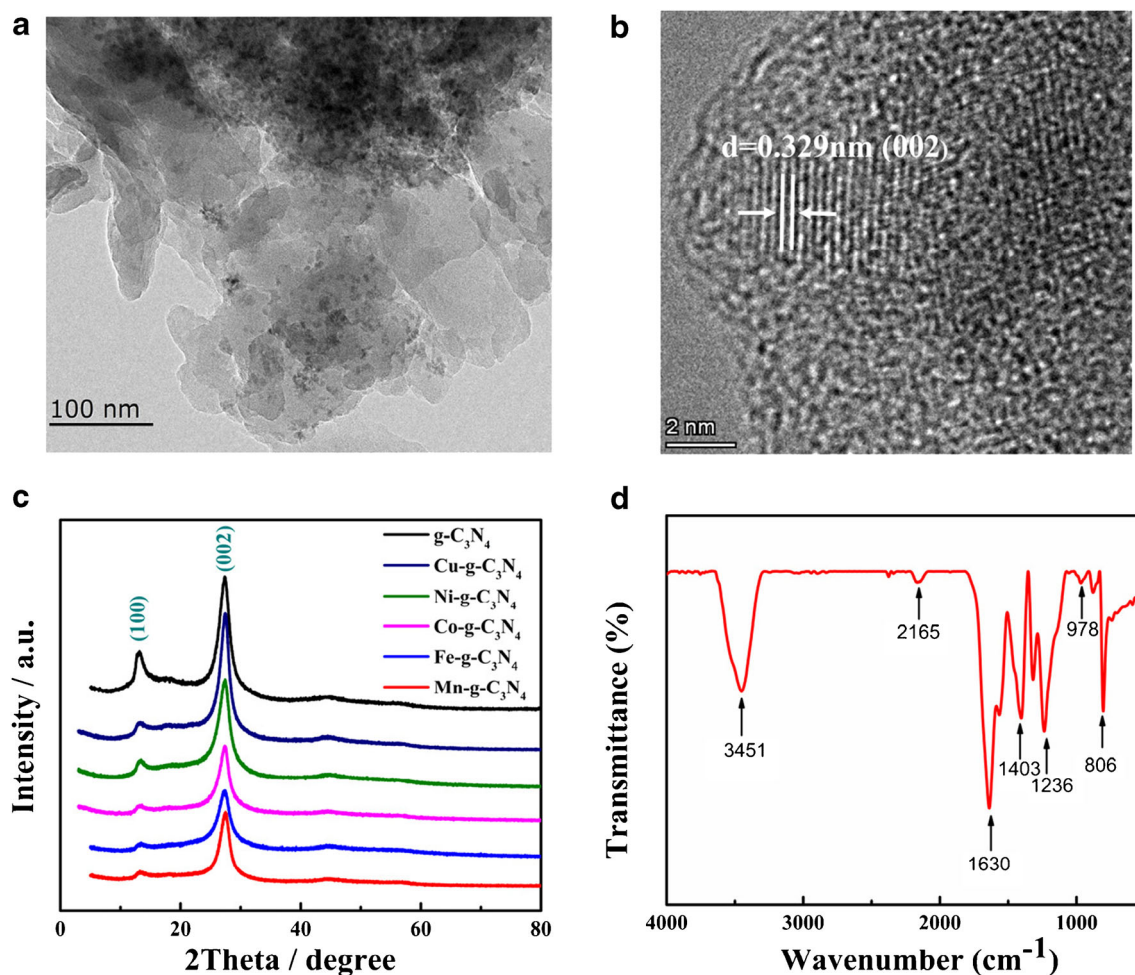


Fig. 2 **a** TEM image of Fe doped $g\text{-C}_3\text{N}_4$ nanoflakes. **b** HR-TEM image of Fe doped $g\text{-C}_3\text{N}_4$ nanoflakes. **c** XRD patterns of $g\text{-C}_3\text{N}_4$ nanoflakes, Cu- $g\text{-C}_3\text{N}_4$, Ni- $g\text{-C}_3\text{N}_4$, Co- $g\text{-C}_3\text{N}_4$, Fe- $g\text{-C}_3\text{N}_4$, Mn- $g\text{-C}_3\text{N}_4$ nanoflakes (from top to bottom). **d** FT-IR image of Fe doped $g\text{-C}_3\text{N}_4$ nanoflakes

In addition, for purpose of exploring the chemical valence and oxidation state information of the elements in the sample of Fe-doped g-C₃N₄ nanoflakes, the XPS spectrum was also performed subsequently and added to curve fit the spectra of N1s and Fe 2p (Fig. 3). A strong absorption peak can be observed at 532.2 eV which can be ascribed to the absorbed H₂O and CO₂ of the sample, which had been confirmed by FT-IR as mentioned above. Two primary peaks with banding energy of 287.6 eV and 284.3 eV appeared in the XPS C1s spectrum (Fig. 3b), the C1s peak at 287.6 eV is relevant to the sp² C-O and tri-s-triazine structures N=C=N bonds of the g-C₃N₄ structure, another absorption peak appeared at 284.8 eV can be associated with the sp² C-C bond, corresponding to C absorbed on the surface of the sample [20, 21]. The obtained N1s spectra of the Fe-doped g-C₃N₄ nanoflakes are decomposed into four species (Fig. 3c), including pyridinic N at 397.7 eV, triazine rings (C-N-C) at 398.6 eV, tertiary N (N-(C)₃, 399.8 eV). And N associated with Fe (Fe-N) also lies in 398.8 ± 0.5 eV, which is too close to the C-N-C unites and difficult to be distinguished [24]. The XPS spectrum of Fe 2p displays two apparent absorption peaks at 710.6 eV and

723.9 eV (Fig. 3D), respectively. Which can be assigned to the characteristic Fe 2p_{3/2} and Fe 2p_{1/2} signals of Fe³⁺ [25–27]. The peak at 709.2 eV is on account of Fe coordinated with N and corresponds to the peak at 398.6 eV [24]. Specifically, six lone pairs of electrons existed in the triazine structure of g-C₃N₄ can take up of the free orbital of the Fe center to build Fe-N moieties, causing a lower electron density accompanied with higher binding energy of the N atom [25, 28]. As we all know that Fe³⁺ carried a higher charge compared with other metal ions (Cu²⁺, Mn²⁺, Co²⁺, Ni²⁺), which can coordinate to the g-C₃N₄ with lone pairs of electrons more easily to some extent. Furthermore, the surface of g-C₃N₄ nanoflakes is negatively charged and the average Zeta potential is −25.1 mV (Fig. S8), which can absorb positively charged metal ions especially Fe³⁺ with more positive charge compared with other metal ions (Cu²⁺, Mn²⁺, Co²⁺, Ni²⁺) [27]. These results that all illustrated Fe-doped g-C₃N₄ nanoflakes displays the highest catalytic properties for the oxidation of TMB among various metal-doped g-C₃N₄, which can be ascribed to the high affinity of Fe³⁺ toward g-C₃N₄ due to Fe-N chemical bond and electrostatic interactions.

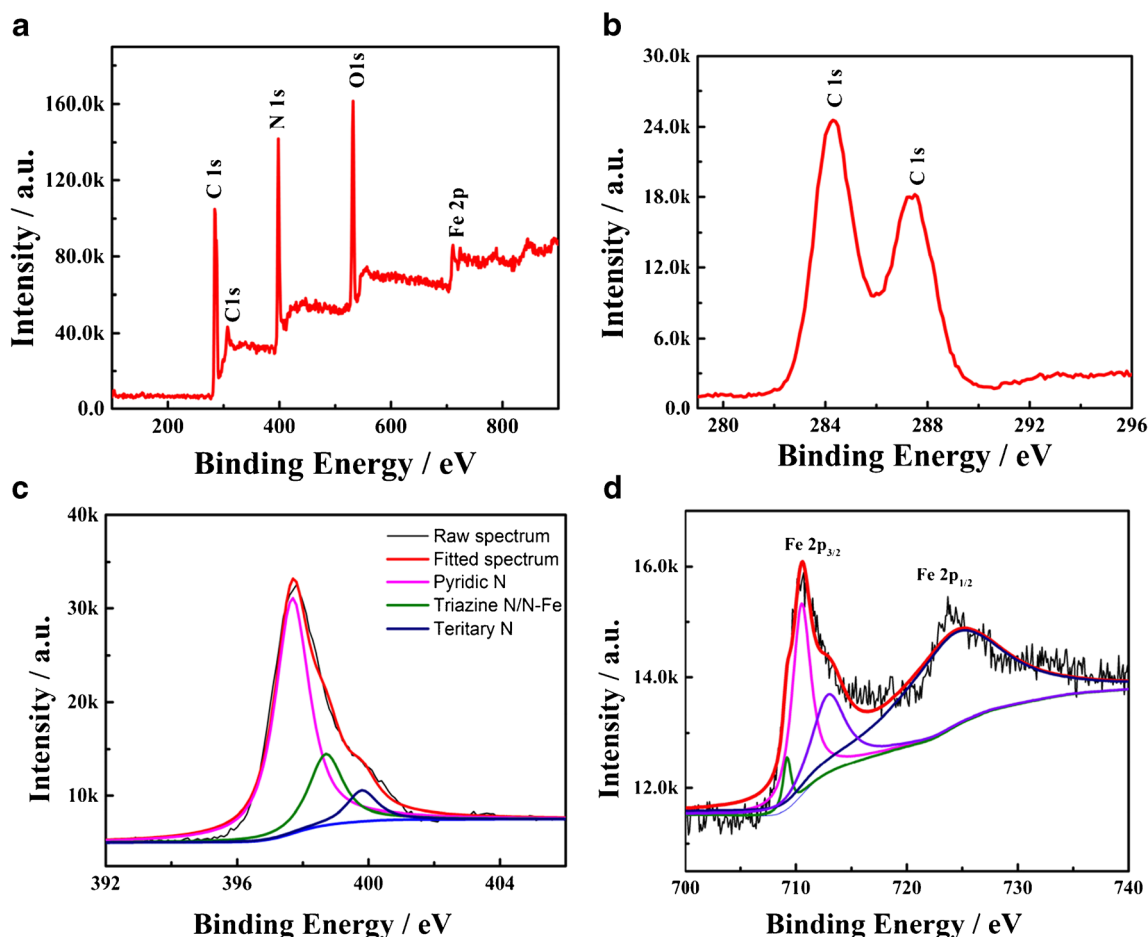


Fig. 3 XPS spectrum of Fe-doped g-C₃N₄ nanoflakes: full survey spectrum (a), C 1s (b), N 1s (c), Fe 2p (d)

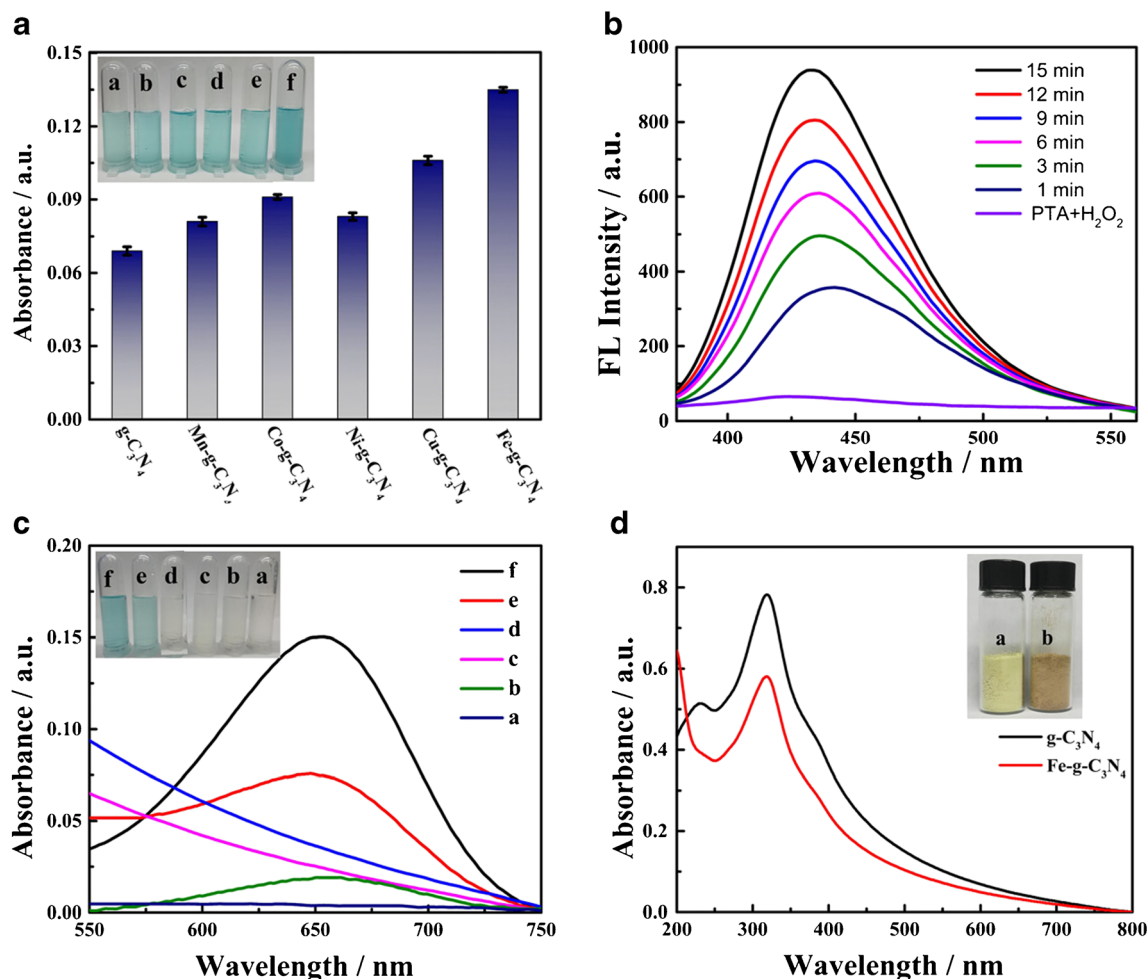


Fig. 4 **a** The absorption spectra with different metals doped $g\text{-C}_3\text{N}_4$ nanoflakes as catalyst in the reaction systems. Inset showed the corresponding final color of different reaction systems. **b** The image of fluorescence intensity over time generated from $\cdot\text{OH}$ of the system which was captured by PTA. **c** The absorption spectra of various reaction systems: TMB (a); $\text{H}_2\text{O}_2 + \text{TMB}$ (b); TMB + $g\text{-C}_3\text{N}_4$ nanoflakes (c); TMB + Fe-doped $g\text{-C}_3\text{N}_4$ nanoflakes (d); $\text{H}_2\text{O}_2 + \text{TMB} + g\text{-C}_3\text{N}_4$

nanoflakes (e); $\text{H}_2\text{O}_2 + \text{TMB} + \text{Fe-doped } g\text{-C}_3\text{N}_4$ nanoflakes (f). Reaction conditions: 0.5 mM TMB, $30 \mu\text{g mL}^{-1}$ catalyst, 0.5 mM H_2O_2 in HAc-NaAc buffer (pH 4.0). Inset were the corresponding pictures of the colored products. **d** UV-Vis spectra of $g\text{-C}_3\text{N}_4$ nanoflakes and Fe-doped $g\text{-C}_3\text{N}_4$ nanoflakes. Inset was the paragraphs of the solid products: $g\text{-C}_3\text{N}_4$ nanoflakes (a); Fe-doped $g\text{-C}_3\text{N}_4$ nanoflakes (b)

The fluorescence spectrum intensities of the $g\text{-C}_3\text{N}_4$ nanoflakes and Fe-doped $g\text{-C}_3\text{N}_4$ nanoflakes were also explored (Fig. S9), and the details can be found in the ESI.

Kinetic investigation of Fe-doped $g\text{-C}_3\text{N}_4$ as peroxidase mimics

For purpose of further exploring the catalytic activities of Fe-doped $g\text{-C}_3\text{N}_4$ nanoflakes, steady-state kinetics was investigated using enzyme kinetics theory with H_2O_2 and TMB as substrates, respectively. Then the Lineweaver-Burk plots were obtained according to the corresponding Michaelis-Menten kinetics data. Michaelis-Menten kinetics equation is displayed as follows:

$$1/V = (K_m/V_{max}) \cdot (1/[S]) + 1/V_{max} \quad (3)$$

The Michaelis constant (K_m) means the obtained concentration of the substrate (S) when the enzymatic reaction arrives to half of the maximum velocity (V_{max}). The smaller the K_m value, the greater affinity of the enzyme to the substrate appeared. V_{max} , another characteristic parameter of the enzyme, represents the maximum velocity during the whole reaction process, from the substrate concentration with time response curve and corresponding Lineweaver-Burk plot, we can conclude the K_m value of Fe-doped $g\text{-C}_3\text{N}_4$ nanoflakes were 0.16 mM with TMB as substrate, and 0.39 mM with H_2O_2 as substrate (Fig. S10). As depicted in Table S1, the value of K_m for the Fe-doped $g\text{-C}_3\text{N}_4$ nanoflakes with H_2O_2 as substrate is much lower than that of the natural horseradish peroxidase (HRP) and other related $g\text{-C}_3\text{N}_4$ nanozymes. The results indicate that Fe-doped $g\text{-C}_3\text{N}_4$ nanoflakes with peroxidase-like activity exhibit a considerable higher affinity

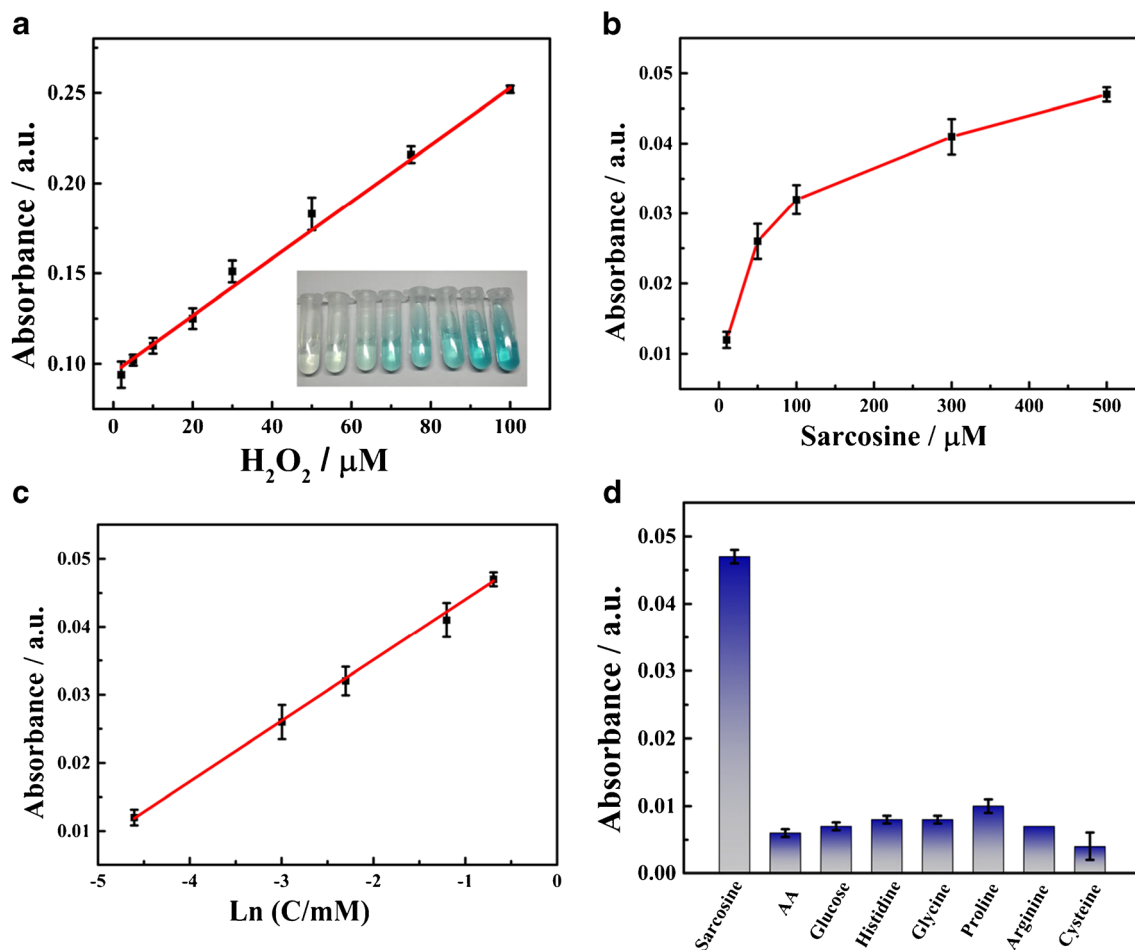


Fig. 5 **a** The linear relationship between the absorbance intensity at 652 nm and the H_2O_2 concentration (2–100 μM , inset: the color change with corresponding concentrations). **b** The relationship between the absorbance at 652 nm and the concentration of sarcosine (10–500 μM).

c The linear relationship between the absorbance intensity at 652 nm and the sarcosine concentrations. **d** The absorbance at 652 nm of the system upon with sarcosine (0.5 mM) and various interfering substances (2.0 mM)

toward H_2O_2 and have an enormous potential application value in the future.

Colorimetric detection of H_2O_2 and discussion of the catalytic mechanism

To investigate the catalytic activity of different metals (Mn, Fe, Co, Ni, Cu)-doped $g-C_3N_4$ nanoflakes toward H_2O_2 -TMB system, we synthesized five types of $g-C_3N_4$ nanoflakes nanozyme materials and compared the catalytic activities of them under the identical conditions. The results showed that Fe-doped $g-C_3N_4$ nanoflakes displayed the highest catalytic

properties for the oxidation of TMB and obtained the darkest blue product solution compared with the others (Fig. 4a).

To further explore the possible peroxidase catalytic mechanism of Fe-doped $g-C_3N_4$ nanozyme, we verified the mechanism of $\bullet OH$ through the fluorescence method. In short, we added terephthalic acid (PTA) to the reaction system as trapping agent of $\bullet OH$, the results illustrated that Fe-doped $g-C_3N_4$ nanozyme can catalyze the decomposition of H_2O_2 to generate $\bullet OH$ efficiently. PTA without fluorescence itself is easily coupled with $\bullet OH$ to form 2-hydroxyterephthalic acid with intense fluorescence, which produces significant blue fluorescence near 430 nm. The fluorescence intensity increased significantly with time in the presence of PTA

Table 1 Reliability of the colorimetric sensing platform in detecting the content of sarcosine in human serum sample

Human serum sample	Add (mM)	Found (mM)	Recovery (%)	RSD ($n = 3$) (%)
1	0.01	0.0095	94.7	5.1
2	0.40	0.3860	96.5	3.5

Table 2 Reliability of the colorimetric sensing platform in detecting the content of sarcosine in urine sample of the patients

Urine Sample	Sarcosine Elisa Kit (μM)	Experimental results (μM)	Added (μM)	Found (μM)	Recovery (%)
1	13.7	14.3	30	39.4	88.9
2	16.1	17.9	30	49.2	102.7

(Fig. 4b). These results confirmed a fact that $\bullet\text{OH}$ are obtained by the decomposition of H_2O_2 with Fe-doped $\text{g-C}_3\text{N}_4$ nanoflakes as catalyst, and promote the oxidation of PTA to generate 2-hydroxyterephthalic acid with blue fluorescence. We also explored the amount of $\bullet\text{OH}$ generated from different systems with different metals (Mn, Fe, Co, Ni, Cu)-doped $\text{g-C}_3\text{N}_4$ nanoflakes as catalyst (Fig. S11), under the same incubation conditions, the system with Fe-doped $\text{g-C}_3\text{N}_4$ nanoflakes exhibited a higher fluorescence intensity compared with other systems, which illustrated Fe-doped $\text{g-C}_3\text{N}_4$ nanoflakes can produce more $\bullet\text{OH}$ compared other four types doped $\text{g-C}_3\text{N}_4$ nanoflakes and possessed excellent catalytic activity among them. The recyclability of the catalyst is studied by a five-run test (Fig. S12), details can be found in the ESI.

For purpose of exploring the catalytic performance of the Fe-doped $\text{g-C}_3\text{N}_4$ nanoflakes, different reaction systems were studied by UV-Vis spectrum (Fig. 4c). In the reaction systems contained only TMB, $\text{g-C}_3\text{N}_4$ nanoflakes or Fe-doped $\text{g-C}_3\text{N}_4$ nanoflakes, no absorption peaks were observed at 652 nm, and colorless solutions were presented to us. In contrast, in the reaction systems that existed both TMB and H_2O_2 , a weak absorption peak at 652 nm with a slight color change could be observed. However, compared with adding $\text{g-C}_3\text{N}_4$ nanoflakes, when added Fe doped $\text{g-C}_3\text{N}_4$ nanoflakes to the same reaction system, a strong absorption peak at 652 nm and an intensively blue solution could be obtained, which explained that the oxidation of TMB is dependent on the synergistic interaction of H_2O_2 and Fe-doped $\text{g-C}_3\text{N}_4$ nanoflakes. The adulteration of Fe^{3+} into $\text{g-C}_3\text{N}_4$ nanoflakes changed the structure and electron distribution and improved its optical and catalytic properties to some extent. This effect can be reflected by the fact that the color change from light yellow for bare $\text{g-C}_3\text{N}_4$ to brown yellow after Fe^{3+} doping (Fig. 4d), and without changing the position of the maximum absorption wavelength, only the intensity of the peak was weakened.

Table 3 An overview on recently reported nanomaterial-based methods for determination of H_2O_2

Methods	Materials	Linear range [μM]	Detection limit [μM]	Ref
Electrochemistry	Grapheme-MWCNT	20–2100	9.4	[29]
Electrochemistry	Multiwalled carbon nanotubes	0.049–22	0.035	[30]
Fluorometry	$\text{Fe}_3\text{O}_4@\text{MnO}_2$	5–150	1.0	[31]
Colorimetric	Carbon dots	0.1–100	0.009	[32]
Colorimetric	Fe-doped $\text{g-C}_3\text{N}_4$	2–100	1.8	This work

According to the ultrahigh catalytic activity of Fe-doped $\text{g-C}_3\text{N}_4$ nanoflakes toward H_2O_2 -TMB reaction system, which made it possible for the sensitive colorimetric detection of H_2O_2 . We could observe a significant increase of the absorbance intensity at 652 nm accompanied with the increasing concentrations of H_2O_2 from 0 μM to 100 μM (Fig. S13). A good linear relationship was exhibited within 2–100 μM H_2O_2 concentration range and the linear equation is $A = 0.095 + 0.0016C$ (μM) ($R^2 = 0.998$); “A” represents the absorbance at 652 nm and “C” on behalf of the various concentrations of H_2O_2 here (Fig. 5A). The limit of detection (LOD = $3\sigma/k$) was calculated as 1.8 μM . Compared with other detection methods reported previously (Table 3), the colorimetric sensor for the detection of H_2O_2 mentioned in this article has a relatively low detection limit and exhibits an excellent catalytic performance toward the TMB- H_2O_2 system, displayed the potential value for further development.

Colorimetric detection of sarcosine

Sarcosine can be oxidized to generate H_2O_2 with the existence of SOX and O_2 (Fig. 1), which made it feasible to further establish a reliable sensing platform to detect sarcosine. A significant increase of the absorbance intensity at 652 nm accompanied with the increasing concentrations of sarcosine from 0 mM to 10 mM was observed (Fig. S14). And a good linear range of 10–500 μM is determined with an adjusted R-square value of 0.9986, the linear equation is $A = 0.0528 + 0.0089\text{LnC}$ (mM) (Fig. 5b, c), ($R^2 = 0.997$). “C” represents the concentration of the sarcosine, and the detection limit ($S/N = 3$) was calculated as 8.6 μM . The possible interfering substances during the detection of sarcosine were also explored to evaluate the specificity to sarcosine of the colorimetric sensor (Fig. 5d), whereas the changes of absorbance intensity at 652 nm upon addition of AA, glucose, histidine, glycine,

Table 4 An overview on recently reported nanomaterial-based methods for determination of sarcosine

Methods	Materials	Linear range [μM]	Detection limit [μM]	Ref
Photoelectrochemical	CuInS ₂	10–1000	8	[33]
Colorimetric	Horseradish peroxidase	1–200	0.7	[34]
Colorimetric	Pd NPs	0.01–50	0.005	[35]
Colorimetric	2D Fe-CTF	10–100	0.56	[36]
Colorimetric	Fe-doped g-C ₃ N ₄	10–500	3.6	This work

proline, arginine, cysteine were negligible nearly. Maybe complex samples can influence the selectivity of the sensor to some extent. However, with the high specificity of SOX toward sarcosine and the satisfactory stability of Fe-doped g-C₃N₄ nanozyme, and as shown in the experimental results above, a real poor response signal was observed in the absence of sarcosine. We can believe that the colorimetric sensor we constructed may have a good selectivity for sarcosine even in complex samples.

In addition, to explore the practicability of our colorimetric sensor, we investigated the sarcosine concentrations in human serum subsequently. Ten folds-diluted concentration of the original serum samples were used in order to ensure that the sarcosine content of the sample is within the standard curve we established. We added 0.01 mM, 0.40 mM sarcosine to the human serum sample, and the recovery percent of this sensing system was calculated in the range of 94% ~ 100% (Table 1). The urine samples obtained from PCa patients were also used to further verify the practicability of the method, the urine samples were centrifuged and diluted to remove the excess impurities and calibrate the concentrations of the sample with the standard Sarcosine Elisa kit, the results were compared with the experimental results we measured. Then, we added 30 μM sarcosine to the urine sample, and the recovery percent of this sensing system was calculated (Table 2). Compared with other detection methods reported previously (Tables 3 and 4), the colorimetric sensor for detecting of sarcosine and H₂O₂ designed in this article has a lower detection limit and exhibits an excellent catalytic performance toward the TMB-H₂O₂ system.

Conclusions

In conclusion, we synthesized a type of Fe-doped g-C₃N₄ nanoflakes with remarkable peroxidase-like activity and constructed a colorimetric sensor for the effective sensing of sarcosine and H₂O₂. And explored the catalytic mechanism of the peroxidase, the catalysts of the decomposition of H₂O₂ to •OH radicals were verified through the fluorescence method. In comparison with other nanomaterials-based methods, our method allows the detection of H₂O₂ and sarcosine within the range of 2–100 μM and 10–500 μM , respectively. More

importantly, this approach can also be introduced to detect sarcosine in both serum and urine samples, and the catalyst has a higher reusable utilization. Although it possess multiple advantages, it is undeniable that the major influence of temperature is the main limitation of this sensor, the reaction temperature and time which need to be controlled strictly during each experiment. And the stability and reproducibility of the sensor have a room for improvement in the future. In a word, we should believe that the colorimetric sensor will have a tremendous potential in the application of disease diagnosis, environmental pollution prevention and other unknown matrices in the near future.

Funding information This work was supported by the General Project Program of the Natural Science Foundation of Hubei Province (no. 2017CFB529), the National Natural Science Foundation of China (grant no. 21405035, 21775033), and the Open Project Funding of the State Key Laboratory of Biocatalysis and Enzyme Engineering.

Compliance with ethical standards

Conflict of interest The author(s) declare that they have no conflict of interest.

References

1. Wu JJ, Wang XY, Wang Q, Lou ZP, Li SR, Zhu YY, Qin L, Wei H (2019) Nanomaterials with enzyme-like characteristics (nanozymes): next-generation artificial enzymes (II). *Chem Soc Rev* 48:1004–1076. <https://doi.org/10.1039/C8CS00457A>
2. Ling PH, Zhang Q, Cao TT, Gao F (2018) Versatile three-dimensional porous cu@Cu₂O aerogel networks as electrocatalysts and mimicking peroxidases. *Angew Chem Int Ed* 57:6819–6824. <https://doi.org/10.1002/anie.201801369>
3. Sun HJ, Zhou Y, Ren JS, Qu XG (2018) Carbon nanozymes: enzymatic properties, catalytic mechanism, and applications. *Angew Chem Int Ed* 57:9224–9237. <https://doi.org/10.1002/anie.201712469>
4. Jin L, Meng Z, Zhang Y, Cai S, Zhang Z, Li C, Shang L, Shen Y (2017) Ultrasmall Pt nanoclusters as robust peroxidase mimics for colorimetric detection of glucose in human serum. *ACS Appl Mater Interfaces* 9:10027–10033. <https://doi.org/10.1021/acsami.7b01616>
5. He WW, Jia HM, Li XX, Lei Y, Li J, Zhao HX, Mi LM, Zhang LZ, Zheng Z (2012) Understanding the formation of CuS concave superstructures with peroxidase-like activity. *Nanoscale*. 4:3501–3506. <https://doi.org/10.1039/C2NR30310H>

6. Jiao L, Wang Y, Jiang HL, Xu Q (2018) Metal–organic frameworks as platforms for catalytic applications. *Adv Mater* 30:1703663. <https://doi.org/10.1002/adma.201703663>
7. Zhang H, Liang X, Han L, Li F (2018) “Non-naked” gold with glucose oxidase-like activity: a nanozyme for tandem catalysis. *Small* 14:1803256. <https://doi.org/10.1002/sml.201803256>
8. Zhang ZJ, Zhang XH, Liu BW, Lin JW (2017) Molecular imprinting on inorganic nanozymes for hundred-fold enzyme specificity. *J Am Chem Soc* 139:5412–5419. <https://doi.org/10.1021/jacs.7b00601>
9. Zhang XL, Zheng C, Guo SS, Li J, Yang HH, Chen G (2014) Turn-on fluorescence sensor for intracellular imaging of glutathione using g-C₃N₄ nanosheet–MnO₂ sandwich nanocomposite. *Anal Chem* 86:3426–3434. <https://doi.org/10.1021/ac500336f>
10. Wang X, Maeda K, Thomas A, Takahane K, Xin G, Carlsson JM, Domen K, Antonietti M (2009) A metal-free polymeric photocatalyst for hydrogen production from water under visible light. *Nat Mater* 8:76–80. <https://doi.org/10.1038/nmat2317>
11. Zhu JJ, Xiao P, Li HL, Carabineiro SAC (2014) Graphitic carbon nitride: synthesis, properties, and applications in catalysis. *ACS Appl Mater Interfaces* 6:16449–16465. <https://doi.org/10.1021/am502925j>
12. Wang YW, Wang LX, An FP, Xu H, Yin ZJ, Tang SR, Yang HH, Song HB (2017) Graphitic carbon nitride supported platinum nanocomposites for rapid and sensitive colorimetric detection of mercury ions. *Anal Chim Acta* 980:72–78. <https://doi.org/10.1016/j.aca.2017.05.019>
13. Zhang WC, Li X, Xu XC, He YF, Qiu FX, Pan JM, Niu XH (2019) Pd nanoparticle-decorated graphitic C₃N₄ nanosheets with bifunctional peroxidase mimicking and ON–OFF fluorescence enable naked-eye and fluorescent dual-readout sensing of glucose. *Mater Chem B* 7:233–239. <https://doi.org/10.1039/C8TB02110D>
14. Cernei N, Heger Z, Gumulec J, Zitka O, Masarik M, Babula P, Eckschlager T, Stiborova M, Kizek R, Adam V (2013) Sarcosine as a potential prostate cancer biomarker—a review. *Int J Mol Sci* 14:13893–13908. <https://doi.org/10.3390/ijms140713893>
15. Cernei N, Zitka O, Ryvolova M, Adam V, Masarik M, Kizek R (2012) Spectrometric and electrochemical analysis of sarcosine as a potential prostate carcinoma marker. *Int J Electrochem Sci* 7:4286–4301
16. Dong WF, Huang YM (2020) CeO₂/C nanowire derived from a cerium(III) based organic framework as a peroxidase mimic for colorimetric sensing of hydrogen peroxide and for enzymatic sensing of glucose. *Microchim Acta* 187:11. <https://doi.org/10.1007/s00604-019-4032-2>
17. Zhang X, Wang CY, Gao YF (2020) Cerium(III)-doped MoS₂ nanosheets with expanded interlayer spacing and peroxidase-mimicking properties for colorimetric determination of hydrogen peroxide. *Microchim Acta* 187:111. <https://doi.org/10.1007/s00604-019-4078-1>
18. Su L, Cai YX, Wang L, Dong WP, Mao GJ, Li Y, Zhao MS, Ma YH, Zhang H (2020) Hemin@carbon dot hybrid nanozymes with peroxidase mimicking properties for dual (colorimetric and fluorometric) sensing of hydrogen peroxide, glucose and xanthine. *Microchim Acta* 187:1–11. <https://doi.org/10.1007/s00604-019-4103-4>
19. Zhang P, Sun DR, Cho A, Weon S, Lee S, Lee J, Han JW, Kim DP, Choi WY (2019) Modified carbon nitride nanozyme as bifunctional glucose oxidase-peroxidase for metal-free bioinspired cascade photocatalysis. *Nat Commun* 10:940. <https://doi.org/10.1038/s41467-019-08731-y>
20. Devi KRS, Mathew S, Rajan R, Georgekutty J, Kasinathan K, Pinheiro D, Sugunan S (2019) Biogenic synthesis of g-C₃N₄/Bi₂O₃ heterojunction with enhanced photocatalytic activity and statistical optimization of reaction parameters. *Appl Surf Sci* 494:465–476. <https://doi.org/10.1016/j.apsusc.2019.07.125>
21. Li Y, Liu XM, Tan L, Cui ZD, Yang XJ, Zheng YF, Yeung KWK, Chu P, Wu SL (2018) Rapid sterilization and accelerated wound healing using Zn²⁺ and graphene oxide modified g-C₃N₄ under dual light irradiation. *Adv Funct Mater* 28:1800299. <https://doi.org/10.1002/adfm.201800299>
22. Liu Q, Guo YR, Chen ZH, Zhang ZG, Fang XM (2016) Constructing a novel ternary Fe (III)/graphene/g-C₃N₄ composite photocatalyst with enhanced visible-light driven photocatalytic activity via interfacial charge transfer effect. *Appl Catal B Environ* 183:231–241. <https://doi.org/10.1016/j.apcatb.2015.10.054>
23. Zhang JS, Zhang MW, Zhang GG, Wang XC (2012) Synthesis of carbon nitride semiconductors in sulfur flux for water photoredox catalysis. *ACS Catal* 2:940–948. <https://doi.org/10.1021/cs300167b>
24. Serov A, Artyushkova K, Atanassov P (2014) Fe-N-C oxygen reduction fuel cell catalyst derived from carbendazim: synthesis, structure, and reactivity. *Adv Energy Mater* 4:1301735. <https://doi.org/10.1002/aenm.201301735>
25. Kim SJ, Mahmood J, Kim CG, Kim SW, Jung S, Zhu G, De Yoreo JJ, Kim G, Baek JB (2018) Defect-free encapsulation of Fe0 in 2D fused organic networks as a durable oxygen reduction electrocatalyst. *J Am Chem Soc* 140:1737–1742. <https://doi.org/10.1021/jacs.7b10663>
26. Hu JS, Zhang PF, An WJ, Liu L, Liang YH, Cui WQ (2019) In-situ Fe-doped g-C₃N₄ heterogeneous catalyst via photocatalysis-Fenton reaction with enriched photocatalytic performance for removal of complex wastewater. *Appl Catal B Environ* 245:130–142. <https://doi.org/10.1016/j.apcatb.2018.12.029>
27. Ye MY, Zhao ZH, Hu ZF, Hu ZF, Liu LQ, Hui MH, Shen ZR, Ma TY (2017) 0D/2D heterojunctions of vanadate quantum dots/graphitic carbon nitride nanosheets for enhanced visible-light-driven photocatalysis. *Angew Chem Int Ed* 56:8407–8411. <https://doi.org/10.1002/anie.201611127>
28. Li HC, Shan C, Pan BC (2018) Fe (III)-doped g-C₃N₄ mediated peroxymonosulfate activation for selective degradation of phenolic compounds via high-valent iron-oxo species. *Environ Sci Technol* 52:2197–2205. <https://doi.org/10.1021/acs.est.7b05563>
29. Woo S, Kim YR, Chung TD, Piao YZ, Kim H (2012) Synthesis of a graphene–carbon nanotube composite and its electrochemical sensing of hydrogen peroxide. *Electrochim Acta* 59:509–514. <https://doi.org/10.1016/j.electacta.2011.11.012>
30. Tavakkoli H, Akhond M, Ghorbankhani GA, Absalan G (2020) Electrochemical sensing of hydrogen peroxide using a glassy carbon electrode modified with multiwalled carbon nanotubes and zein nanoparticle composites: application to HepG₂ cancer cell detection. *Microchim Acta* 187:105. <https://doi.org/10.1007/s00604-019-4064-7>
31. Zhu WY, Zhou Y, Tao MD, Yan XQ, Liu Y, Zhou XM (2020) An electrochemical and fluorescence dual-signal assay based on Fe₃O₄@MnO₂ and N-doped carbon dots for determination of hydrogen peroxide. *Microchim Acta* 187:187. <https://doi.org/10.1007/s00604-020-4163-5>
32. Gul U, Kanwal S, Tabassum S, Gilani MA, Rahim A (2020) Microwave-assisted synthesis of carbon dots as reductant and stabilizer for silver nanoparticles with enhanced-peroxidase like activity for colorimetric determination of hydrogen peroxide and glucose. *Microchim Acta* 187:135. <https://doi.org/10.1007/s00604-019-4098-x>
33. Jiang XY, Zhang L, Liu YL, Yu XD, Liang YY, Qu P, Zhao WW, Xu JJ, Chen HY (2018) Hierarchical CuInS₂-based heterostructure:

- application for photocathodic bioanalysis of sarcosine. *Biosens Bioelectron* 107:230–236. <https://doi.org/10.1016/j.bios.2018.02.039>
34. Yamkamon V, Phakdee B, Yainoy S, Suksrichawalit T, Tatanandana T, Sangkum P, Eiamphungporn W (2018) Development of sarcosine quantification in urine based on enzyme-coupled colorimetric method for prostate cancer diagnosis. *EXCLI J* 17:467. <https://doi.org/10.17179/excli2018-145>
35. Lan JM, Xu WM, Wan QP, Zhang X, Lin J, Chen JH, Chen JZ (2014) Colorimetric determination of sarcosine in urine samples of prostatic carcinoma by mimic enzyme palladium nanoparticles. *Anal Chim Acta* 825:63–68. <https://doi.org/10.1016/j.aca.2014.03.040>
36. Su LJ, Zhang Z, Xiong YH (2018) Water dispersed two-dimensional ultrathin Fe (iii)-modified covalent triazine framework nanosheets: peroxidase like activity and colorimetric biosensing applications. *Nanoscale* 10:20120–20125. <https://doi.org/10.1039/C8NR06907G>

Publisher's note Springer Nature remains neutral with regard to jurisdictional claims in published maps and institutional affiliations.